



ELSEVIER

Earth and Planetary Science Letters 192 (2001) 423–438

EPSL

www.elsevier.com/locate/epsl

Cenozoic structural and metamorphic evolution of the eastern Himalayan syntaxis (Namche Barwa)

Lin Ding^a, Dalai Zhong^a, An Yin^{b,*}, Paul Kapp^b, T. Mark Harrison^b

^a *Institute of Geology and Geophysics, LTE Lab, Chinese Academy of Sciences, Beijing 100029, PR China*

^b *Department of Earth and Space Sciences and Institute of Geophysics and Planetary Physics, University of California, Los Angeles, CA 90095-1567, USA*

Received 10 May 2001; received in revised form 24 July 2001; accepted 25 July 2001

Abstract

Combined geological and geochronological investigations of the eastern Himalayan syntaxis in the Namche Barwa region of Tibet reveal the first-order elements of its Cenozoic tectonic evolution. The syntaxis is characterized by a northeast-plunging antiform and is bounded by two northeast-striking strike-slip shear zones: a left-slip shear zone on the western side and a right-slip shear zone on the eastern side. These strike-slip shear zones are linked by east–west-trending thrusts and served either as (1) a roof thrust to a large duplex system or (2) transfer faults to a south-directed thrust system that accommodated northward indentation of a folded Indian plate. An east–west-trending pop-up structure in the core of the antiform juxtaposes a granulite-bearing complex over sillimanite-bearing gneisses of Gangdese affinity to the north and of Indian affinity to the south. Previous studies suggest that mafic granulites in the complex record at least two episodes of metamorphism at $\sim 800^\circ\text{C}$: the first at high pressures (14–15 kbar) followed by a second event at 8–10 kbar. Zircons from mafic granulites yield four populations of concordant U–Pb ion microprobe ages. Two groups are at ~ 65 Ma and ~ 160 Ma, and likely crystallized during Andean-type Gangdese magmatism prior to the Indo-Asian collision. A third cluster at ~ 40 Ma exhibits very low Th/U ratios, and is interpreted to have crystallized in the presence of fluids associated with a high-pressure granulite facies metamorphic event during the early stages of the Indo-Asian collision, subsequent to high-pressure metamorphism in the western Himalaya syntaxis between ~ 50 and 43 Ma. A fourth cluster of zircons yields ages between 11 and 25 Ma and Th/U ratios that decrease systematically with decreasing age. We interpret the youngest zircon age (~ 11 Ma) to represent the timing of moderate-pressure high-grade metamorphism, with the older ages and higher Th/U ratios being a result of mixing with a restitic igneous component. This interpretation, coupled with a ~ 8 Ma $^{40}\text{Ar}/^{39}\text{Ar}$ age on hornblende from a metadiorite within the core of the antiform, suggests that the Namche Barwa syntaxis has been characterized by rapid cooling and exhumation since at least Late Miocene time. Despite its contrasting structural setting, the Miocene and younger metamorphism and cooling history in the Namche Barwa syntaxis are strikingly similar to those of the Nanga Parbat syntaxis of the western Himalaya. © 2001 Elsevier Science B.V. All rights reserved.

Keywords: Qinghai-Xizang Plateau; Himalayan Orogeny; duplexes; thrust faults

* Corresponding author. Tel.: +1-310-825-8752; Fax: +1-310-825-2779. *E-mail address:* yin@ess.ucla.edu (A. Yin).

1. Introduction

The 2000 km long, east–west-trending Himalayan orogenic belt terminates at the Nanga Parbat syntaxis in the west and the Namche Barwa syntaxis in the east [1,2] (Fig. 1). The Himalayan orogen has been dominated by north–south contraction during the Cenozoic Indo-Asian collision [3–5], although at times this phase of deformation has been coeval with north–south and east–west extension [6–8]. In contrast to dominantly dip-slip faulting along the Himalayan orogen, strike-slip tectonics prevail east and west of the two Himalayan syntaxes. West of the Nanga Parbat syntaxis, the Chaman fault system has accommodated northward motion of India with respect to Afghanistan and Iran via left-slip motion (e.g. [9,10]). East of the Namche Barwa syntaxis, right-slip faults dominate along the Indo-Burman ranges [11] and along the northern edge of the Indochina block (i.e. the Red River fault system [12,13]). In addition to the fact that the Hima-

layan syntaxes define the boundaries between contrasting tectonic regimes, the syntaxes also define the location of the two largest rivers (Indus and Yalu Tsangpo) that transport sediments from the Tibetan plateau. The high denudation rates associated with these rivers have raised the possibility that erosional processes may have provided a positive feedback mechanism for localizing large-magnitude crustal deformation [1,2].

Exposures of granulite to eclogite facies rocks within the Himalayan syntaxes [14–16] provide unique opportunities to study the deep crustal composition and processes occurring during the Indo-Asian collision. Recent studies of the Nanga Parbat syntaxis suggest that its rapid uplift since the Late Miocene [17] can be in part attributed to a local feedback between tectonic and surface processes [2], namely east–west contraction along a north-trending crustal-scale pop-up structure [18,19] coupled with large-magnitude river incision. Whether or not this conclusion can be extrapolated to the much less studied Namche Bar-

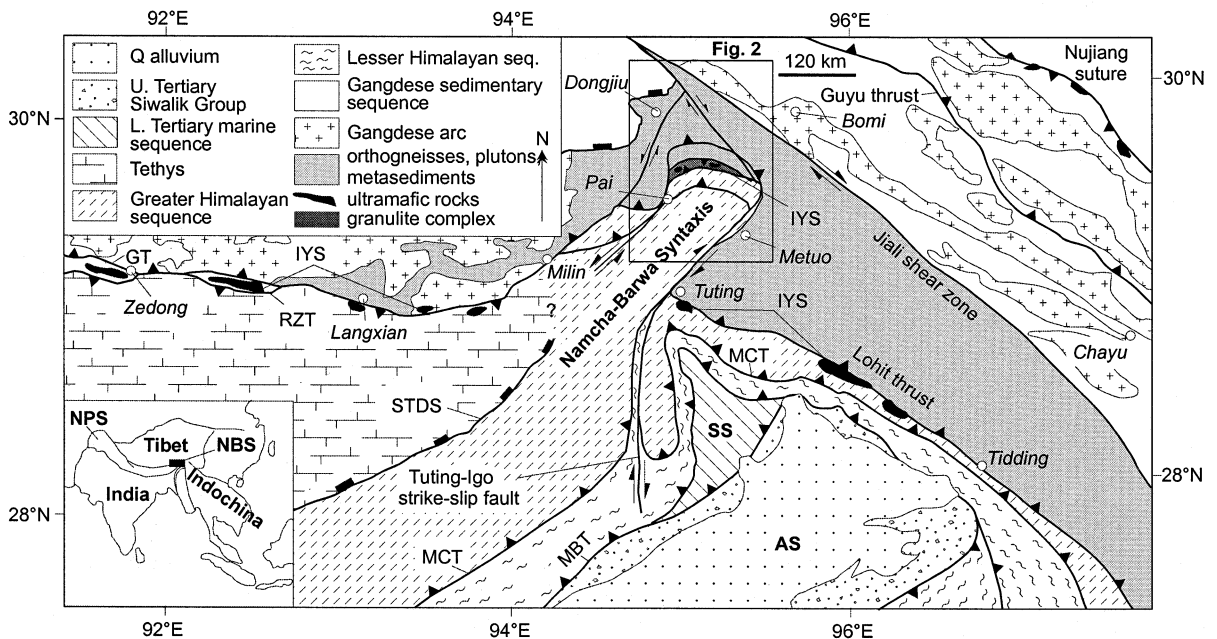


Fig. 1. Geological sketch map of the eastern Himalayan syntaxis (Namche Barwa) and surrounding regions. Abbreviations: AS, Assam syntaxis; GT, Gangdese thrust; IYS, Indus–Yalu suture; MBT, Main Boundary thrust; MCT, Main Central thrust; NBS, Namche Barwa syntaxis; NPS, Nanga Parbat syntaxis; RZT, Renbu–Zedong thrust; SS, Siang syntaxis; STDS, South Tibet Detachment System.

wa syntaxis remains uncertain. Although rapid denudation during the Pliocene–Pleistocene has been documented for the Namche Barwa syntaxis [1,20,21], the earlier history of granulite facies metamorphism and exhumation has not been constrained.

In order to understand the tectonic development of the Namche Barwa syntaxis, a geologic mapping project with emphasis on characterizing structural styles and fault kinematics was conducted building upon earlier studies in the region [1,20–22]. We describe east–west-trending thrust zones in the high-grade core of the Namche Barwa antiform that are linked with a left-slip shear zone to the west and a right-slip shear zone to the east. These shear zones either may represent a large duplex system that was exhumed by subsequent folding or served as transfer systems that accommodated northward indentation of a previously folded Indian plate. The field study was integrated with $^{40}\text{Ar}/^{39}\text{Ar}$ thermochronometry and U–(Th)–Pb ion microprobe zircon analyses to constrain the timing of metamorphism and deformation in this region. Results of U–(Th)–Pb zircon studies on Namche Barwa granulites suggest that Indian continental crust was underthrust beneath Asia to a depth of ~ 55 km by ca. 40 Ma, and that high-grade metamorphism in the eastern Himalayan syntaxis was occurring as recently as ~ 11 Ma. These results are compatible with collision between India and Asia prior to 40 Ma at the eastern end of the Himalaya and rapid cooling of Namche Barwa rocks since Late Miocene time.

2. Geology of the Namche Barwa syntaxis

Although strongly modified by the Gangdese and Renbu–Zedong thrusts [23–25], the trace of the Indus–Yalu suture (IYS) can be recognized in southeastern Tibet by a series of ophiolite fragments along the Yalu Tsangpo valley (Fig. 1). West of Namche Barwa, the suture separates the Cretaceous–Tertiary Gangdese batholith of the Asian plate in the north from the Tethyan Himalayan sequence of the Indian plate in the south. East of the Namche Barwa syntaxis, metamorphosed ophiolite fragments northeast of Tuting

are suggested to be the eastward continuation of the IYS [1,26,27] (Fig. 1). The ophiolite fragments separate the eastern extension of the Gangdese batholith to the north from Indian gneisses to the south. Here, the Tethyan Himalayan sequence is absent and must have been either completely denuded [26,27] or underthrust beneath the batholith to the north. Within the Namche Barwa antiform, a granulite-bearing complex containing ultramafic fragments has been regarded as a deep crustal exposure of the IYS [28] (Fig. 2).

The overall structure of the Namche Barwa syntaxis is a large north-plunging antiform [1,22]. This crustal-scale fold is outlined by a south-facing U-shaped shear zone system that consists of multiple strands of ductile thrusts and strike-slip shear zones (Figs. 1 and 2). The western boundary of the massif is defined by the sillimanite-bearing left-slip Pai mylonitic shear zone that exhibits subhorizontal stretching lineations. This shear zone appears to link with the north-dipping Yarlung–Tsangpo Canyon thrust zone to the north, which juxtaposes metasedimentary rocks, orthogneisses, and plutons of Gangdese affinity in the hanging wall over sillimanite-bearing gneisses, mafic amphibolites, and minor marble in its footwall (Fig. 2). The east–west-trending segment of the Yarlung–Tsangpo Canyon thrust makes a sharp turn at its eastern end and links with the northeast–southwest-trending Aniqiao right-slip shear zone (Fig. 2). The Aniqiao shear zone and the northeast-trending segment of the Yarlung–Tsangpo Canyon thrust form a broad right-slip shear zone that bounds the eastern side of the Namche Barwa antiform (Fig. 2). The IYS is separated right-laterally by ~ 120 km across the Aniqiao shear zone (Fig. 1).

Inside the U-shaped fault system in the northern part of the Namche Barwa antiform is a large pop-up structure (Fig. 2), which is bounded by the north-dipping Namu–La thrust in the south and the south-dipping Langjiapo thrust in the north. The Namu–La thrust places sillimanite gneisses on top of kyanite gneisses. Both of the latter units belong to the Greater Himalayan Crystalline rocks, which elsewhere in the Himalaya form the hanging wall of the Main Central Thrust. The Namu–La Thrust exhibits both brit-

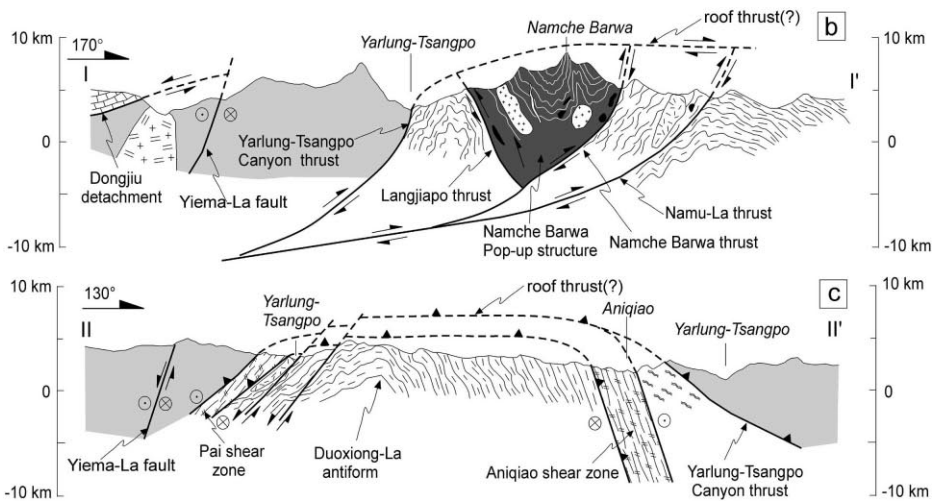
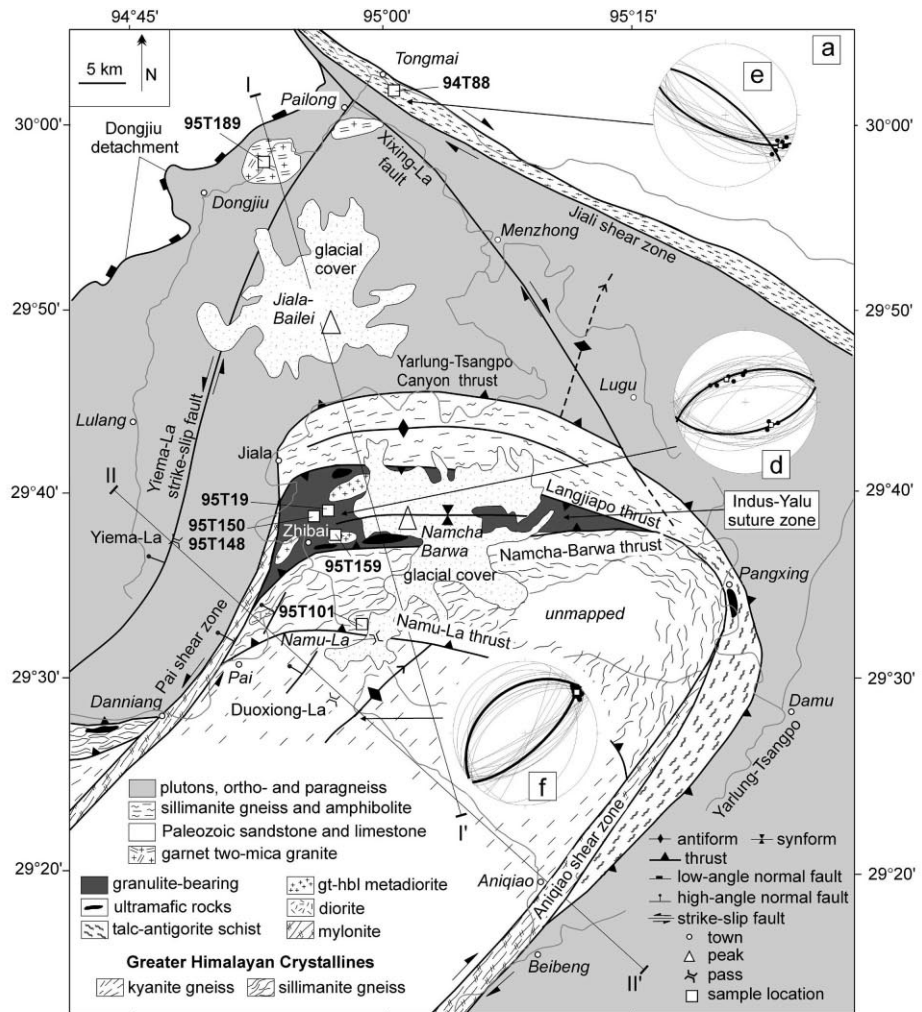


Fig. 2. Geologic map (a) and cross-sections (b and c) of the Namche Barwa syntaxis based on mapping at a scale of 1:100000. Lower hemisphere, equal-area stereographic projections of measured foliation planes and lineation trends within the (d) core of the Namche Barwa pop-up structure, (e) Jiali strike-slip fault zone, and (f) Duoxiong–La antiform.

tle and ductile deformation. The south-dipping Langjiapo thrust is expressed by a 2 km thick zone of mylonitic orthogneiss, which juxtaposes an ultramafic- and granulite-bearing metamorphic complex in the hanging wall to the south over sillimanite gneisses and mafic amphibolites in the footwall to the north (Fig. 2). The presence of mafic amphibolites distinguishes the footwall rocks from the Indian sillimanite gneisses to the south, and may imply that they are of Gangdese affinity.

The granulite-bearing complex in the hanging wall of the Langjiapo thrust forms a small

wedge-shaped pop-up structure that narrows eastward (Fig. 2). Its southern boundary is the north-dipping Namche Barwa thrust that juxtaposes the granulite-bearing complex over Greater Himalayan sillimanite gneisses of the Indian plate. The granulite complex is characterized by pelitic gneisses, in some places migmatitic, that include meter-scale boudins of ultramafic and mafic lithologies. The peak metamorphic assemblage observed for pelitic gneiss is garnet+kyanite+rutile+feldspar+quartz. The boudins of ultramafic rocks west of the Namche Barwa peak near Zhibai (Fig. 2a) contain the mineral assemblage: olivine+or-

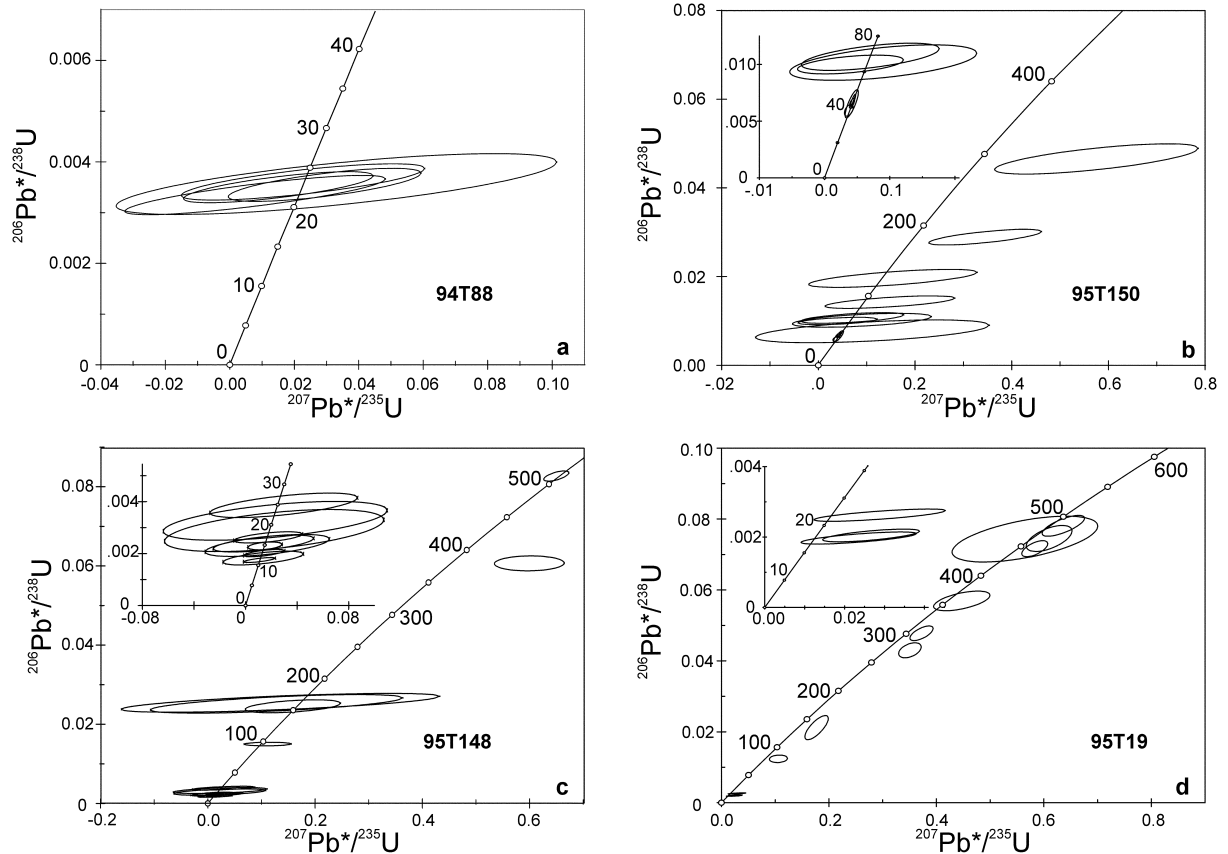


Fig. 3. Concordia diagram showing U–Pb ion microprobe zircon ages. Insets are concordia diagrams showing the younger ages. Error ellipses are shown at 2σ uncertainty.

Table 1
U–Th–Pb isotopic data

Spot ID	Isotopic ratios			$^{207}\text{Pb}^*/^{206}\text{Pb}^*$	$\pm 1\sigma$	Th/U	$^{206}\text{Pb}^*$ (%)	Apparent ages $\pm 1\sigma$ (Ma)		$^{207}\text{Pb}^*/^{206}\text{Pb}^*$
	$^{206}\text{Pb}^*/^{238}\text{U}$	$\pm 1\sigma$	$^{207}\text{Pb}^*/^{235}\text{U}$					$\pm 1\sigma$	$^{206}\text{Pb}^*/^{238}\text{U}$	
94T88 Garnet-bearing two-mica leucogranite										
r7g1s1 ^a	3.50e-03	1.25e-04	1.51e-02	1.20e-02	2.40e-02	6.74e-01	96.2	22.5 ± 0.8	15 ± 12	neg
r7g2s1 ^a	3.35e-03	1.58e-04	7.85e-03	1.65e-02	3.50e-02	4.05e-01	93.4	21.5 ± 1.0	8 ± 17	neg
r7g3s1 ^a	3.56e-03	2.45e-04	3.31e-02	2.79e-02	6.73e-02	6.55e-01	88.1	22.9 ± 1.6	33 ± 27	846 ± 1650
r7g6s1 ^a	3.55e-03	1.33e-04	2.94e-02	1.22e-02	6.01e-02	7.61e-01	95.5	22.8 ± 0.9	29 ± 12	608 ± 842
r7g7s1 ^a	3.61e-03	1.46e-04	2.27e-02	1.54e-02	4.57e-02	4.99e-01	93.4	23.2 ± 0.9	23 ± 15	neg
95T150 Garnet–pyroxene granulite										
r13g3s1 ^a	4.65e-02	1.39e-03	5.75e-01	8.59e-02	1.17e-02	2.53e-01	95.2	293 ± 9	461 ± 55	1418 ± 249
r13g4s1 ^b	9.99e-03	3.38e-04	3.98e-02	3.32e-02	2.89e-02	2.97e-02	86.9	64.1 ± 2.2	40 ± 32	neg
r13g4s2 ^b	1.07e-02	4.90e-04	7.03e-02	4.32e-02	4.78e-02	2.09e-02	87.9	68.4 ± 3.1	69 ± 41	89 ± 1400
r13g8s1 ^a	2.89e-02	7.23e-04	3.45e-01	4.74e-02	8.66e-02	3.29e-02	95.1	184 ± 5	301 ± 36	1351 ± 233
r13g16s1 ^b	1.02e-02	6.39e-04	9.00e-02	5.86e-02	6.43e-02	2.18e-02	83.2	65.1 ± 4.1	88 ± 55	750 ± 1310
r13g17s1 ^a	1.42e-02	5.75e-04	1.48e-01	5.47e-02	2.60e-02	4.25e-02	86.5	91 ± 4	140 ± 48	1077 ± 693
r13g18s1 ^a	1.96e-02	8.28e-04	1.54e-01	7.10e-02	2.47e-02	1.98e-02	89.6	125 ± 5	146 ± 62	492 ± 957
r13g18s2 ^b	7.67e-03	1.05e-03	1.12e-01	9.86e-02	1.06e-01	7.76e-02	68.6	49.2 ± 6.7	108 ± 90	1726 ± 1500
r2g3s1 rim ^b	6.85e-03	2.11e-04	4.38e-02	1.60e-03	4.64e-02	2.69e-03	99.5	44.0 ± 1.4	44 ± 2	18 ± 45
r2g3s2 core ^b	6.63e-03	1.55e-04	4.22e-02	1.57e-03	4.62e-02	5.70e-04	99.7	42.6 ± 1.0	42 ± 2	9 ± 69
r2g4s1 core ^b	6.53e-03	5.07e-04	4.17e-02	4.13e-03	4.63e-02	3.83e-03	99.4	42.0 ± 3.2	42 ± 4	15 ± 137
r2g4s2 rim ^b	5.96e-03	2.09e-04	3.72e-02	2.76e-03	4.53e-02	1.13e-03	98.9	38.3 ± 1.3	37 ± 3	neg
95T148 Garnet–pyroxene granulite										
r1g1s1 ^a	2.89e-03	3.31e-04	2.22e-02	3.47e-02	5.56e-02	5.46e-02	69.2	19 ± 2	22 ± 34	437 ± 3370
r1g1s2 core ^a	3.26e-03	3.05e-04	2.30e-02	3.54e-02	5.10e-02	5.61e-02	74.3	21 ± 2	23 ± 35	242 ± 3450
r1g1s3 rim ^a	1.83e-03	1.08e-04	1.36e-02	1.26e-02	5.41e-02	2.96e-03	83.8	12 ± 12	14 ± 13	375 ± 2000
r1g2s1 ^a	2.02e-03	5.72e-05	1.44e-02	6.30e-03	5.17e-02	8.53e-03	91.9	13 ± 1	15 ± 6	271 ± 962
r1g3s1 ^a	2.39e-03	1.33e-04	1.39e-02	1.58e-02	4.21e-02	4.38e-02	84.6	15 ± 1	14 ± 16	neg
r1g5s1 ^a	2.32e-03	1.73e-04	1.68e-02	1.96e-02	5.27e-02	3.48e-02	81.2	15 ± 1	17 ± 20	314 ± 2560
r1g6s1 ^a	3.86e-03	1.92e-04	2.95e-02	2.33e-02	5.54e-02	1.30e-02	86.9	25 ± 1	29 ± 23	427 ± 1690
r1g8s1 rim ^a	1.75e-03	3.85e-05	1.07e-02	4.78e-03	4.42e-02	2.22e-03	93.6	11 ± 1	11 ± 5	neg
r1g8s2 core ^a	2.63e-03	8.75e-05	1.75e-02	1.07e-02	4.83e-02	2.03e-02	90.3	17 ± 1	18 ± 11	115 ± 1403
r1g8s3 ^a	2.30e-03	6.08e-05	1.50e-02	5.31e-03	4.73e-02	6.03e-03	94.5	15 ± 1	15 ± 5	66 ± 821
r1g7s1 ^b	1.50e-02	1.81e-04	1.12e-01	1.76e-02	5.39e-02	7.42e-02	97.0	96 ± 1	107 ± 16	367 ± 337
r1g7s2 ^b	8.27e-02	5.28e-04	6.50e-01	9.46e-03	5.70e-02	6.32e-01	99.7	512 ± 3	508 ± 6	490 ± 27
r1g9s1 ^b	2.52e-02	9.59e-04	1.28e-01	9.59e-02	3.69e-02	6.48e-01	90.1	160 ± 6	122 ± 86	neg
r1g9s2 core ^b	2.54e-02	9.72e-04	1.35e-01	1.21e-01	3.86e-02	6.90e-01	89.2	162 ± 6	129 ± 109	neg
r1g9s3 rim ^b	2.46e-02	6.66e-04	1.59e-01	3.61e-02	4.69e-02	4.66e-01	96.5	156 ± 4	150 ± 32	41 ± 526
r1g4s1 ^b	6.07e-02	7.69e-04	6.00e-01	2.65e-02	7.17e-02	5.04e-02	98.7	380 ± 5	477 ± 17	977 ± 85.3
95T19 Muscovite-bearing leucogranite vein										
r2g1s1 ^a	7.81e-02	1.20e-03	6.36e-01	1.61e-02	5.91e-02	nm	100.0	485 ± 7	500 ± 10	570 ± 38
r2g1s2 rim ^a	7.45e-02	1.50e-03	6.10e-01	1.74e-02	5.93e-02	nm	100.0	463 ± 9	483 ± 11	579 ± 51

Table 1 (continued)

Spot ID	Isotopic ratios				Th/U	$^{206}\text{Pb}^*/^{206}\text{Pb}^*$	$^{206}\text{Pb}^*/^{238}\text{U}$	Apparent ages $\pm 1\sigma$ (Ma)	
	$^{206}\text{Pb}^*/^{238}\text{U} \pm 1\sigma$	$^{207}\text{Pb}^*/^{235}\text{U} \pm 1\sigma$	$^{207}\text{Pb}^*/^{206}\text{Pb}^*$	$\pm 1\sigma$				$^{206}\text{Pb}^*/^{238}\text{U}$	$^{207}\text{Pb}^*/^{235}\text{U}$
r2g2s1 ^a	4.30e-02	8.62e-04	3.51e-01	8.61e-03	5.92e-02	1.42e-03	271 \pm 5	305 \pm 6	573 \pm 52
r2g3s1 ^a	2.05e-03	7.35e-05	2.66e-02	4.95e-03	9.45e-02	1.55e-02	13 \pm 1	27 \pm 5	1518 \pm 309
r2g3s2 ^a	1.97e-03	7.01e-05	2.35e-02	5.90e-03	8.66e-02	1.96e-02	13 \pm 1	24 \pm 6	1351 \pm 436
r2g4s1 ^a	4.78e-02	8.47e-04	3.72e-01	8.82e-03	5.65e-02	1.02e-03	301 \pm 5	321 \pm 7	472 \pm 40
r2g5s1 ^a	2.12e-02	1.39e-03	1.77e-01	8.88e-03	6.06e-02	2.63e-03	135 \pm 9	165 \pm 8	626 \pm 94
r2g6s1 ^a	5.69e-02	1.13e-03	4.47e-01	2.14e-02	5.70e-02	2.28e-03	357 \pm 7	375 \pm 15	491 \pm 88
r2g7s1 ^a	7.44e-02	2.64e-03	5.65e-01	5.54e-02	5.51e-02	4.59e-03	462 \pm 16	455 \pm 36	416 \pm 186
r2g8s1 ^a	7.17e-02	9.25e-04	5.83e-01	9.88e-03	5.90e-02	7.96e-04	446 \pm 6	467 \pm 6	568 \pm 29
r2g9s1 ^a	2.62e-03	7.11e-05	2.88e-02	6.71e-03	7.97e-02	1.70e-02	17 \pm 1	29 \pm 7	1188 \pm 422
r2g9s2 ^a	1.24e-02	4.28e-04	1.06e-01	6.84e-03	6.21e-02	4.31e-03	79 \pm 3	102 \pm 6	676 \pm 149

^a Radiogenic Pb, corrected for common Pb, neg, negative apparent age due to reverse discordance; nm, not measured.

^a Corrected for common Pb using measured ^{204}Pb .

^b Corrected for common Pb using measured ^{208}Pb and Th/U.

thopyroxene + phlogopite + spinel \pm hornblende \pm clinopyroxene, whereas the mafic boudins contain the peak metamorphic assemblage: garnet+clinopyroxene+rutile+quartz \pm orthopyroxene \pm plagioclase. Thermobarometric studies on the pelitic and mafic granulites yield steep clockwise P – T paths. Peak metamorphic assemblages equilibrated at high pressures (> 14 kbar at $\sim 800^\circ\text{C}$) [15,20]. A second episode of granulite facies metamorphism is recorded in mafic samples by symplectites of orthopyroxene+clinopyroxene+plagioclase after garnet, which yield pressures between 8 and 10 kbar and temperatures of 800–900°C [20]. The most recently crystallized amphibolite facies mineral assemblages equilibrated at 600–800°C and 5.5–7 kbar in pelitic samples [15] and 650–700°C and 4.5–6 kbar in mafic samples [20].

Gneisses within the granulite complex are interpreted to be of Indian affinity [1]. The mafic boudins within the gneiss, however, contain inherited Jurassic–Cretaceous zircons (see results presented below), suggesting an affinity to the Gangdese arc. This mixture of Indian and Gangdese rocks observed in the granulite-bearing complex supports the previous interpretation that it represents the suture zone between India and Asia [28]. Ultramafic boudins in the granulite complex could represent fragments of either Tethyan oceanic mantle or mantle lithosphere that was beneath the Gangdese arc.

Ductile shear zones to the north of Namche Barwa include the NW-striking right-slip Jiali mylonitic shear zone and the north-dipping Dongjiu detachment fault. The Jiali shear zone has been considered as the easternmost strand of the Karakorum–Jiali fault zone, a large active right-slip fault system across central Tibet [29]. The Jiali shear zone is subvertical and exhibits subhorizontal stretching lineations (Fig. 2e). It juxtaposes Paleozoic sandstones and limestones intruded by Gangdese granitoids to the north from Gangdese orthogneisses to the south. The Dongjiu fault is a low-angle normal fault that juxtaposes Gangdese orthogneisses and mylonitic schists in the footwall against Gangdese Ordovician to Permian sedimentary sequences in the hanging wall (Figs. 1 and 2). This fault may be the eastern continuation of the South Tibetan detachment system [6,30].

Table 2
Summary of $^{40}\text{Ar}/^{39}\text{Ar}$ results

Temperature °C	$^{40}\text{Ar}/^{39}\text{Ar}$	$^{36}\text{Ar}/^{39}\text{Ar}$	$^{37}\text{Ar}/^{39}\text{Ar}$	$^{38}\text{Ar}/^{39}\text{Ar}$	$^{39}\text{Ar}_K$ (10^{-12} mol)	$(^{40}\text{Ar}^{2a}/^{39}\text{Ar})$	$^{39}\text{Ar}_k^a$	Age (Ma)
95T159 Hornblende ($J=0.01038$; weight = 0.35 g)								
450	35.48	0.1202	4.902	0.2019	0.24	0.47 ± 0.12	0.45	8.8 ± 3.0
650	27.88	0.0936	4.718	0.2357	0.47	0.67 ± 0.09	0.88	12.4 ± 2.0
800	18.48	0.0609	3.528	0.1565	0.53	0.81 ± 0.06	0.99	15.2 ± 1.0
950	4.177	0.0111	0.991	0.0541	1.97	0.93 ± 0.02	3.68	17.4 ± 0.6
1050	3.197	0.0078	1.086	0.0489	3.41	0.95 ± 0.02	6.37	17.7 ± 0.6
1100	2.622	0.0059	0.878	0.0387	5.34	0.93 ± 0.02	9.97	17.4 ± 0.6
1160	1.953	0.0038	1.669	0.0419	9.86	0.94 ± 0.01	18.4	17.6 ± 0.5
1220	1.609	0.0024	1.013	0.0295	21.8	0.95 ± 0.01	40.7	17.8 ± 0.5
1280	2.919	0.0070	1.275	0.0495	8.58	0.92 ± 0.02	16.0	17.2 ± 0.6
1340	35.19	0.1185	9.544	0.2547	0.37	1.03 ± 0.11	0.69	19.3 ± 2.0
1400	33.42	0.1105	4.308	0.3842	0.44	1.21 ± 0.12	0.82	22.6 ± 3.0
1500	33.78	0.1111	2.428	0.1911	0.51	1.25 ± 0.13	0.95	23.2 ± 4.0
95T101 Hornblende ($J=0.01068$, weight = 0.25 g)								
520	329.7	1.1216	4.207	0.3514	0.06	0.18 ± 0.02	0.2	3.48 ± 0.21
700	171.8	0.5856	7.176	0.2909	0.09	0.19 ± 0.03	0.3	3.59 ± 0.23
800	220.6	0.7500	2.449	0.2059	0.11	0.20 ± 0.04	0.36	3.78 ± 0.3
900	147.8	0.5029	4.826	0.2754	0.12	0.29 ± 0.06	0.37	5.62 ± 0.4
1000	23.03	0.7273	1.367	0.1727	1.10	0.40 ± 0.07	3.54	7.76 ± 0.5
1150	38.85	0.1314	2.557	0.2346	1.30	0.39 ± 0.03	4.2	7.51 ± 0.3
1300	2.589	0.0086	4.624	0.0250	28.10	0.42 ± 0.02	90.4	8.10 ± 0.2
1500	137.9	0.4655	1.539	0.2672	0.19	1.14 ± 0.04	0.63	21.8 ± 3.8
95T189 Muscovite ($J=0.010378$; weight = 0.30 g)								
460	5.603	0.0195	5.718	0.3298	0.65	0.28 ± 0.02	0.41	5.2 ± 0.4
640	4.413	0.0153	5.250	0.2629	0.99	0.30 ± 0.02	0.62	5.6 ± 0.3
780	6.049	0.0216	8.481	0.2562	0.75	0.32 ± 0.02	0.47	6.0 ± 0.4
860	7.987	0.0262	2.912	0.1299	1.11	0.47 ± 0.03	0.69	8.9 ± 0.5
950	3.663	0.0105	1.221	0.0756	1.99	0.65 ± 0.01	1.25	12.1 ± 0.3
1050	2.585	0.0059	0.601	0.0283	3.69	0.84 ± 0.01	2.30	15.7 ± 0.2
1150	1.210	0.0010	0.149	0.0132	18.8	0.88 ± 0.01	11.7	16.4 ± 0.3
1250	1.022	0.0005	0.054	0.0128	47.3	0.83 ± 0.01	29.5	15.6 ± 0.2
1350	1.059	0.0005	0.020	0.0022	82.1	0.87 ± 0.01	51.1	16.3 ± 0.3
1480	4.963	0.0126	0.480	0.0378	3.13	1.27 ± 0.05	1.96	23.5 ± 0.9

All quoted uncertainties are 1σ .

^aPercentage of cumulative ^{39}Ar released during step heating ($^{40}\text{Ar}/^{39}\text{Ar})_K = 3.05 \times 10^{-2}$, ($^{36}\text{Ar}/^{37}\text{Ar})_{Ca} = 2.64 \times 10^{-4}$, ($^{39}\text{Ar}/^{37}\text{Ar})_{Ca} = 6.87 \times 10^{-4}$.

However, a significant difference exists between the two. The South Tibetan detachment system lies entirely within the Indian plate south of the Indus–Tsangpo suture in the Himalayas, whereas the Dongjiu detachment occurs north of the suture within the Gangdese batholith. As discussed below, the development of the Dongjiu fault and the South Tibetan detachment system may have overlapped in time, and thus the two could have formed coevally under the same stress regime.

The NW-striking right-slip Xixing–La fault and

the NE-striking left-slip Yiema–La fault north of the Namche Barwa syntaxis appear to be active based on their topographic expressions. However, their initiation ages are unknown. They form a conjugate fault system that accommodates both north–south contraction and east–west extension. Active northeast-striking normal faults are present on the west side of the Namche Barwa syntaxis, as expressed by offsets of Yarlung Tsangpo terraces and steep fault scarps. These normal faults may have initiated at ~ 5 Ma [1,21].

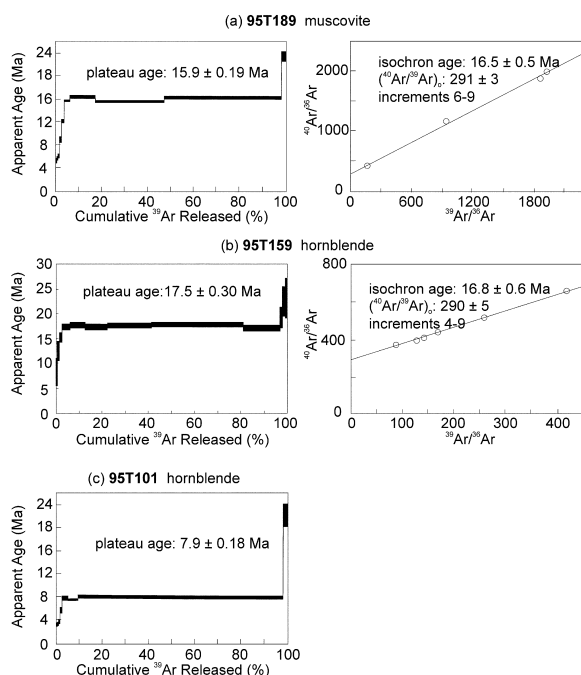


Fig. 4. $^{40}\text{Ar}/^{39}\text{Ar}$ release spectra and isochron diagrams.

3. Geochronologic results and interpretation

Application of U–(Th)–Pb and $^{40}\text{Ar}/^{39}\text{Ar}$ methods provides constraints on the timing of deformation and metamorphism within the eastern Himalayan syntaxis. U–(Th)–Pb single spot analyses on zircon were obtained using the UCLA CAMECA ims 1270 ion microprobe. Zircon separates were obtained from samples collected from outcrop using standard mineral separation techniques. They were mounted in epoxy, polished, and coated with ~ 400 Å of Au. The relative sensitivity factor for U and Pb was obtained using a calibration curve defined by measurement of standard zircon AS-3 (1099.1 ± 0.5 Ma [31]). Most analyses were corrected for common Pb using measured ^{204}Pb . However, for some analyses with favorable Th/U ratios, it was preferable to correct for common Pb using measured ^{208}Pb and assuming concordance between the U–Pb and Th–Pb systems (Table 1). The composition of common Pb was estimated from the model of Stacey and Kramers [32]. Additional details of the U–Pb analytical methods are given in [33]

and [25]. U–(Th)–Pb results are tabulated in Table 1 and shown graphically as concordia plots in Fig. 3.

Minerals analyzed by the $^{40}\text{Ar}/^{39}\text{Ar}$ method were separated using conventional techniques and hand-picked to be $\sim 99\%$ pure. Separates were irradiated for 43 h at the Beijing Nuclear Research Institute Reactor. Also irradiated were Fish Canyon sanidine (27.8 Ma) to calculate J factors and K_2SO_4 and CaF_2 to determine correction factors for interfering neutron reactions. Argon isotope analyses were conducted on a RGA-10 mass spectrometer in the Laboratory of Isotope Geochronology at the Institute of Geology and Geophysics, Chinese Academy of Sciences, Beijing. All samples were step-heated using a radio-frequency furnace. Additional analytical details and data reduction methods are given in [34,35]. Argon isotopic results are summarized in Table 2 and shown graphically as age spectra and isochron plots in Fig. 4.

3.1. Timing of slip along the Jiali fault zone

Sample 94T88 is a garnet- and two-mica-bearing leucosome collected from within the Jiali right-slip shear zone (Fig. 2a). It occurs as a 1–5 m thick vein that is oriented subparallel to the mylonitic fabric of the shear zone. As it is not mylonitized, but exhibits a weak foliation that is concordant with the shear zone, the leucosome may have crystallized during late stages of slip. Five zircons from this leucosome yield concordant U–Pb ages with statistically indistinguishable $^{206}\text{Pb}^*/^{238}\text{U}$ apparent ages (Table 1, Fig. 3a). We interpret the weighted mean $^{206}\text{Pb}^*/^{238}\text{U}$ age of 22.6 ± 0.3 Ma (1σ , $\text{MSWD} = 0.4$) for the five analyses to be the crystallization age for the leucogranite. This result implies that the Jiali shear zone was active before and perhaps at ca. 23 Ma, significantly earlier than the Pliocene age for fault initiation estimated by Armijo et al. [29,36] for the Karakorum–Jiali fault zone.

3.2. Age constraints on the Dongjiu detachment

Sample 95T189 is an undeformed, garnet-bearing two-mica granite that intrudes a mylonitic

shear zone in the footwall of the Dongjiu detachment (Fig. 2a). Muscovite from this granite yields a $^{40}\text{Ar}/^{39}\text{Ar}$ age spectrum with a plateau age of 15.9 ± 0.2 Ma and an isochron age of 16.5 ± 0.5 Ma (Table 2; Fig. 4a). This result provides a minimum age of crystallization for the undeformed granite and suggests that at least the ductile phase of mylonitic gneiss development in this portion of the detachment shear zone was active prior to ca. 16 Ma. This age constraint implies that the Dongjiu fault could have been coeval with the South Tibetan detachment system, which was active between ~ 20 and 10 Ma (e.g. [37–39]).

3.3. U–Pb geochronology of mafic granulites

U–(Th)–Pb ion microprobe analyses were conducted on zircons separated from two different garnet–clinopyroxene mafic granulite boudins (~ 1 m by 0.5 m) that occur within garnet–kyanite gneiss. The boudins are variably retrograded to garnet+hornblende+plagioclase \pm biotite, with the degree of retrogradation increasing toward their margins. Sample 95T150 was collected just west of Namche Barwa peak (Fig. 2a). It is only weakly retrograded, consisting mainly of subequal amounts of garnet and clinopyroxene. Zircons from this sample yield concordant to discordant U–Pb ion microprobe ages (Table 1, Fig. 3b). Precision of the individual analyses relates largely to the U content of the zircon, and thus to the fraction of radiogenic Pb. There are two clusters of concordant zircon ages. The older cluster includes three spot analyses on two different zircons that yield a weighted mean $^{206}\text{Pb}^*/^{238}\text{U}$ age of 65.5 ± 1.3 Ma (1σ , MSWD=0.6). The younger concordant cluster, defined by four spot analyses (two sets of core and rim analyses on two different grains, r2g3 and r2g4), yield $^{206}\text{Pb}^*/^{238}\text{U}$ ages between 38 and 44 Ma, with the rim and core analyses yielding statistically indistinguishable ages. The two grains are prismatic (aspect ratio of $\sim 4:1$) but exhibit either rounded or embayed terminations. The zircon, r2g4, contains abundant inclusions of plagioclase, quartz, and rutile. Sample 95T148 is strongly retrograded to the assemblage garnet+hornblende+plagioclase, and was collected ~ 50 m from sample 95T150. Zircons analyzed

from this sample are euhedral, with an aspect ratio of $\sim 3:1$, and exhibit moderately rounded terminations. There is a cluster of concordant zircons between 11 and 25 Ma (10 spot analyses on six different grains), and two single zircons yield concordant ages of ~ 160 Ma (three spot analyses on one grain) and ~ 510 Ma (Table 1; Fig. 3c).

To better interpret the significance of the populations of concordant zircon ages within the two granulites, we plotted Th/U ratios of all the zircon spot analyses versus their $^{206}\text{Pb}^*/^{238}\text{U}$ ages (Fig. 5). A zircon crystallized from a melt with a Th/U ratio of 4 (typical of the Gangdese batholith [25]) and with partition coefficients determined for zircon by Mahood and Hildreth [40], would be expected to exhibit a Th/U ratio of 0.1–1. However, Th/U ratios generally increase in rocks during granulite facies metamorphism [41], implying that U is preferentially leached relative to Th and that associated metamorphic fluids are characterized by low Th/U. Thus, the Th/U ratio of zircon crystallizing in equilibrium with an aqueous metamorphic fluid is expected to be substantially lower than that crystallizing in equilibrium with a magmatic fluid.

In general, the Th/U ratios of zircons in each sample decrease with younger $^{206}\text{Pb}^*/^{238}\text{U}$ ages. For sample 95T150, the Th/U ratios of the ca. 40 Ma zircons (0.0006–0.004) are one to two orders of magnitude lower than all other analyses, which range between 0.02 and 0.25. This observation, together with the composition of inclusions in r2g4, argues strongly that the ca. 40 Ma age of the youngest zircons represents the age of a granulite–facies metamorphic event. The age significance of the ca. 65 Ma zircons is less clear, as they provide Th/U ratios that are significantly higher but still significantly lower than what would be expected from a zircon crystallized from a typical Gangdese magma. We attribute the ca. 65 Ma crystallization of zircons to Gangdese-type plutonism, with their Th/U ratios being influenced by mixing with ca. 40 Ma metamorphic zircon. Likewise, for sample 95T148, we interpret the concordant zircon at ~ 160 Ma to have crystallized during Gangdese-type magmatism due to its high Th/U ratios (~ 0.5 – 0.7) and the youngest zircons (~ 11 Ma) with the lowest Th/U ratios to

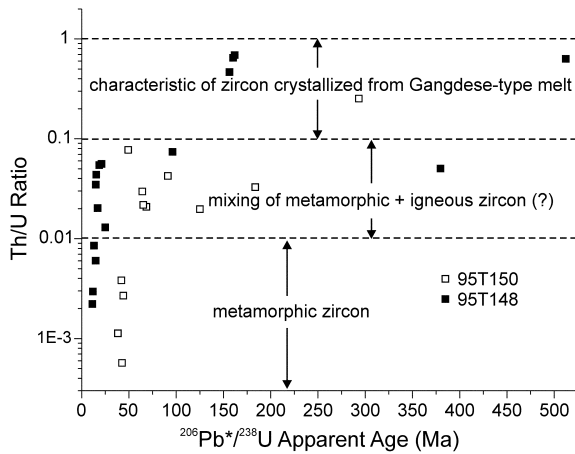


Fig. 5. Plot of Th/U ratios versus $^{206}\text{Pb}^*/^{238}\text{U}$ apparent ages for zircon analyses from two samples of mafic granulites. Note that within each sample, Th/U ratios decrease with decreasing $^{206}\text{Pb}^*/^{238}\text{U}$ age. See text for discussion.

have crystallized during another high-grade metamorphic event. The older Cenozoic zircons, although concordant, exhibit systematically higher Th/U ratios and can be explained by spot analyses that sampled a mix of ~ 11 Ma metamorphic zircon and Mesozoic zircon of igneous origin. The two inferred high-grade metamorphic events at ~ 40 Ma and ~ 11 Ma may correspond, respectively, to the high-pressure and moderate-pressure high-grade metamorphic events suggested from thermobarometric studies. Further studies are needed to evaluate whether high-grade metamorphism was continuous or episodic within the Namche Barwa syntaxis during the time interval between 11 and 40 Ma.

Discordant U–Pb ages for zircons from both granulite samples can be explained by inherited Proterozoic to earliest Paleozoic zircons that experienced either Pb loss or were overgrown by zircon during Mesozoic or Cenozoic time. The concordant U–Pb age of ~ 510 Ma for a zircon in sample 95T148 demonstrates inheritance of early Paleozoic zircons in these granulites that are common in both Himalayan and Tibetan gneisses and sediments (e.g. [1,42–46]).

3.4. Timing of granulite exhumation

Previous K–Ar ages obtained on samples from

the Namche Barwa syntaxis range from ~ 1.2 to > 30 Ma, with ages generally getting older away from the Namche Barwa pop-up structure [22]. These ages and their distribution with respect to the core of the syntaxis are roughly similar to those exhibited by $^{40}\text{Ar}/^{39}\text{Ar}$ biotite ages from the Nanga Parbat syntaxis (see compilation in [18]). New constraints on the higher temperature cooling history of the core of the Namche Barwa syntaxis are provided by $^{40}\text{Ar}/^{39}\text{Ar}$ analyses on hornblende separated from a metadiorite within the Namche Barwa pop-up structure. Sample 95T159 is a garnet–hornblende metadiorite that occurs within the granulite complex (Fig. 2a). Hornblende from this sample yields a $^{40}\text{Ar}/^{39}\text{Ar}$ age spectrum with an apparent plateau age of 17.5 ± 0.3 Ma and an isochron age of 16.8 ± 0.6 Ma (Table 2; Fig. 4b). This result suggests that this portion of the granulite complex cooled to below $\sim 500^\circ\text{C}$ by middle Miocene time, prior to the most recent granulite facies metamorphic event inferred from our U–Th–Pb zircon studies. This discrepancy may be explained by either very high rates of differential rock cooling within the core of the syntaxis due to tectonic juxtaposition or the presence of excess Ar in the hornblende.

Sample 95T101 is a metadiorite located just north of the Namu–La thrust (Fig. 2). Amphibole separated from this sample yields a $^{40}\text{Ar}/^{39}\text{Ar}$ plateau age of 7.9 ± 0.2 Ma (Table 2; Fig. 4c), and suggests cooling of this metadiorite to below the closure temperature for hornblende ($525 \pm 25^\circ\text{C}$; [47]) by this time. This temperature time point, coupled with the proposed high-grade metamorphism ($800 \pm 100^\circ\text{C}$) at ~ 11 Ma implies cooling rates between 50 and $100^\circ\text{C}/\text{Ma}$ for the core of the Namche Barwa syntaxis during Late Miocene time (Fig. 6). Note that sample 95T159 was excluded from this analysis for the reasons discussed in the preceding paragraph. This range in cooling rates is similar to that suggested for the Namche Barwa syntaxis during the Pliocene–Pleistocene from lower-temperature thermochronometric studies [1,21] (Fig. 6).

3.5. Timing of anatexis

U–Th–Pb ages of 3.3–3.9 Ma for xenotime

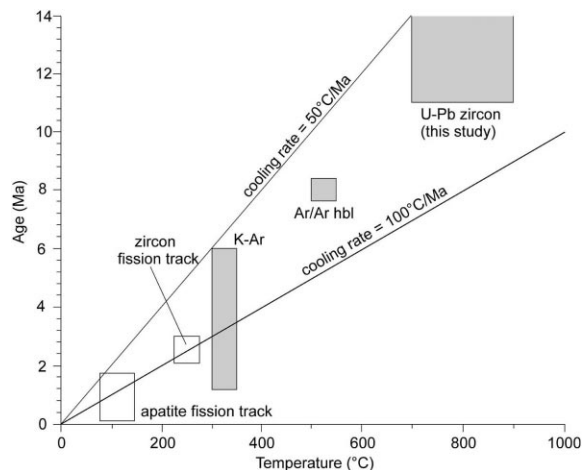


Fig. 6. Age versus temperature plot summarizing thermo-chronologic results from the Namche Barwa syntaxis. Apatite and zircon fission track ages are from [1]. K–Ar ages are from [22]. Open rectangles are results for rocks in the core of the Duoxiong–La antiform; shaded rectangles are results for the Namche Barwa pop-up block.

from a leucosome within the core of the Duoxiong–La antiform are the only existing constraints on the age of Cenozoic anatexis within the Namche Barwa syntaxis [1]. We conducted U–Pb ion microprobe zircon studies on sample 95T19, a weakly deformed leucosome (0.1–0.5 m in width) collected from within the granulite complex (Fig. 2). Zircons yield slightly discordant ages that exhibit a range of $^{206}\text{Pb}^*/^{238}\text{U}$ ages between 13 and 485 Ma (Table 1; Fig. 3d). The analyses lie along a discordia line with an upper intercept of ca. 550 Ma and a lower intercept age that is younger than the youngest $^{206}\text{Pb}^*/^{238}\text{U}$ age of 13 Ma. We suggest that the youngest $^{206}\text{Pb}^*/^{238}\text{U}$ age of 13 Ma provides a maximum crystallization age for the leucosome. This result is compatible with Miocene and younger anatexis within the Namche Barwa syntaxis, which in turn may be related to decompression melting during rapid denudation. The upper intercept age of ca. 550 Ma confirms, again, the remobilization of early Paleozoic material within the Cenozoic Himalayan orogen.

4. Discussion

4.1. The architecture of the Namche Barwa syntaxis

The Indian plate has been subducted beneath the Himalaya along the north-dipping Main Himalayan thrust [48,49] and along the east-dipping subduction zone beneath the Indo-Burman ranges [11]. The crustal-scale Namche Barwa antiform is located in the transition zone where the change in the dip direction of the subducting Indian lithosphere occurs (Fig. 1). Based on this general tectonic setting, Burg et al. [1] suggested that north-east-trending folding has controlled the exhumation and development of the Namche Barwa syntaxis. Although crustal folding may have been an important mechanism in the formation of the eastern Himalayan syntaxis, this process alone cannot explain the observation that granulite facies metamorphic rocks are localized within a narrow east-trending zone bounded by north- and south-dipping thrusts.

Recently, Zeitler et al. [2] proposed a model that emphasizes the role of erosion in localizing strain in the Himalaya orogen. They noted that the highest-grade regional metamorphism occurs where orogen-scale rivers (Indus and Yarlung Tsangpo) cut across the Himalayan belt. Based on this observation, they suggest that the young and rapid exhumation at both the Nanga Parbat and Namche Barwa syntaxes were induced by erosion. Although our studies do not address the role of erosion in controlling tectonism, they do suggest that the structural styles of the two Himalayan syntaxes are markedly different. In the Namche Barwa syntaxis, north–south contraction is important in the axial zone of the north-trending antiform as expressed by the pop-up structure associated with the Langjiapo and Namche Barwa thrusts (Fig. 2). The pop-up structure must be younger than 11 Ma, which is the youngest age of the high-grade metamorphic rocks in the pop-up block. The exhumation of at least portions of the pop-up block from $\sim 525^\circ\text{C}$ to the surface should have occurred after ~ 8 Ma as constrained by the $^{40}\text{Ar}/^{39}\text{Ar}$ hornblende age of a metadiorite within it. Thus, the

pop-up structure is clearly associated with Cenozoic deformation after the initial collision between India and Asia. In contrast, the major contractional structures in the Nanga Parbat syntaxis are all north–south-trending and are dominated by a large east-dipping reverse fault [18,19]. The difference in style of deformation between the eastern and western syntaxes may be due to their differences in boundary conditions. The free-slip boundary condition along the eastern margin of Asia and the proximity of the syntaxis to the oceanic subduction zone beneath Burma may have produced a constrictional strain field that resulted in synchronous east–west extension and north–south contraction. In contrast, the presence of large landmass west of the western syntaxis produces a no-slip boundary condition that has prohibited east–west extension.

Another important difference between the architecture of the Namche Barwa and Nanga Parbat syntaxes is that the major shear zones that are parallel to the syntaxis antiform in the eastern syntaxis are all strike-slip shear zones in their present orientations (i.e. the left-slip Pai and right-slip Aniqiao shear zones). There are two possibilities for the present geometry and kinematics of the two major strike-slip shear zones on both sides of the Namche Barwa antiform. First, the shear zones could have been segments of the north-dipping Yarlung–Tsangpo Canyon thrust that were later folded by the north-trending Namche Barwa antiform (Fig. 7a). This interpretation implies that the pop-up structure at the core of the antiform was part of a large duplex system with the Yarlung Canyon, Pai and Aniqiao shear zones as its roof fault. This raises an interesting possibility that the formation of the Namche Barwa antiform resulted from development of a duplex structure beneath it. Alternatively, the left-slip Pai and the right-slip Aniqiao shear zones are transfer structures linking the Rengbu-Zedong, Lohit, and Yarlung Canyon thrusts, which resulted from northward indentation of the folded Indian crust (Figs. 1 and 7b). The apparent offset of ophiolitic fragments by the Pai and the Aniqiao shear zones and the straight trace of the Jiali shear zone (Fig. 1), which was active prior to and possibly at ~ 23 Ma, appears

to favor the indentation model. It is likely that both mechanisms have operated, either sequentially or coevally, during the formation of the Namche Barwa antiform.

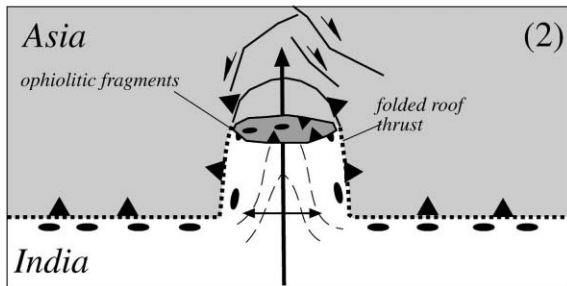
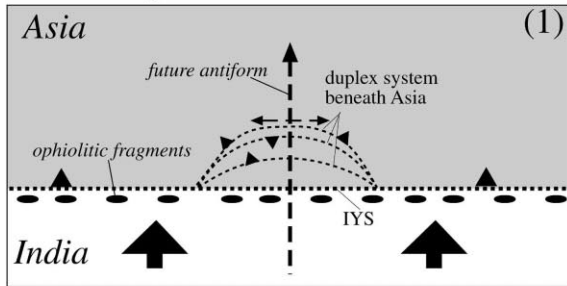
4.2. Age and significance of granulite formation

A scenario that we suggest is most consistent with the regional geology and U–(Th)–Pb zircon studies on the Namche Barwa granulites is as follows. The dated mafic granulites represent a basal portion of the Gangdese continental arc that crystallized during magmatism at ca. 160 and 65 Ma. This interpretation suggests that continental collision between India and Asia at the eastern Himalayan syntaxis initiated after 65 Ma. The basal portion of the Gangdese arc underwent high-pressure granulite facies metamorphism at ca. 40 Ma, which we relate to crustal thickening during the early stages of the Indo-Asia collision. This age of high-pressure metamorphism is slightly younger than that within the western Himalayan syntaxis (~ 43 – 50 Ma [14,50]) and supports a diachronous collision between India and Asia (that it first started in the western syntaxis and propagated to the east [51,52]). The youngest zircons (~ 11 Ma) in the mafic granulites crystallized during an episode of moderate-pressure high-grade metamorphism that was contemporaneous with or shortly predated rapid denudation and anatexis within the Namche Barwa syntaxis. Interestingly, Late Miocene (6–11 Ma) crystallization of zircon in the presence of metamorphic fluids has also been documented within gneisses of the Nanga Parbat syntaxis [53,54].

5. Summary

Field mapping reveals the first-order structural framework of the Namche Barwa syntaxis at the eastern end of the Himalayan orogen, which is significantly different from the style of deformation in the Nanga Parbat syntaxis at the western end of the Himalaya. The syntaxis is dominated by a north-trending antiform and is bounded by two north-striking strike-slip shear zones: a left-slip shear zone on the west side and a right-slip

A. Folding of Both India and Asia



B. Folded India Indenting into Asia

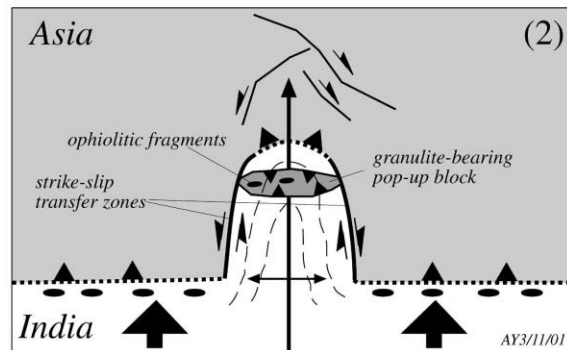
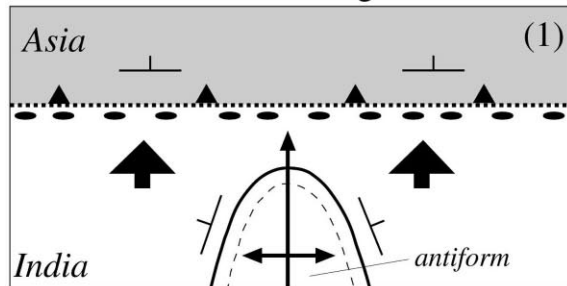


Fig. 7. Two end-member models for the development of the present structural configuration of the Nanche Barwa syntaxis. (a) The strike-slip Pai and Aniqiao shear zones and the Yarlung–Tsangpo Canyon thrust were parts of the same shear zone that served as a roof thrust to a duplex system beneath the Asian margin. This duplex system was later folded by the north-trending Namche Barwa antiform. (b) Alternatively, the left-slip Pai and the right-slip Aniqiao shear zones were transfer structures linking a north-dipping thrust system as represented by the Lohit and the Yarlung Canyon thrusts. This transfer system may have accommodated northward indentation of India, which was folded previously into a northeast-trending antiform.

shear zone on the east side. The core of the antiform is characterized by an east–west-trending pop-up structure that is linked with the aforementioned strike-slip shear zones; together they may be part of a large duplex system responsible for the formation of the Namche Barwa antiform or a transfer fault system that accommodated northward indentation of a previously folded Indian plate. The pop-up block includes granulite facies metamorphic rocks that contain zircons with multiple populations of concordant U–Pb ion microprobe ages. Mesozoic populations are clustered around 160 and 65 Ma, and may represent magmatic events in the Andean-type Gangdese arc prior to the Indo-Asian collision. Evaluation of Th/U ratios of concordant Cenozoic zircons in the granulites suggests high-grade metamorphic events at ~ 40 and ~ 11 Ma. The above age interpretations suggest that rapid denudation rates have characterized the Namche Barwa syntaxis since Late Miocene time and supports the early suggestion that the initial Indo-Asian collision was diachronous across the Himalayan orogen.

Acknowledgements

We thank M.A. Murphy and J.L. D'Andrea (UCLA) for assistance with U–Pb ion microprobe analyses. This work was supported by a grant from the Chinese National Key Project (1998040800), China Natural Science Foundation (Grant 49732100), and the US NSF grants awarded to A. Yin and T.M. Harrison. We acknowledge facility support from the Instrumenta-

tion and Facilities Program of the US NSF. We thank C.E. Manning, Michael Taylor, Eric Cowgill, Martin Hand, and Margaret Rusmore for constructive comments on an early draft of this manuscript. The final manuscript benefited from reviews by Jean-Pierre Burg, Page Chamberlain, and Meg Streepey. *[RV]*

References

- [1] J.-P. Burg, P. Nievergelt, F. Oberli, D. Seward, P. Davy, J.-C. Maurin, Z. Diao, M. Meier, The Namche Barwa syntaxis: evidence for exhumation related to compressional crustal folding, *J. Asian Earth Sci.* 16 (1998) 239–252.
- [2] P.K. Zeitler, A.S. Meltzer, P.O. Koons, D. Craw, B. Hallet, C.P. Chamberlain, W.S.F. Kidd, S.K. Park, L. Seeber, M. Bishop, J. Shroder, Erosion, Himalayan geodynamics, and the geomorphology of metamorphism, *GSA Today* 11 (2001) 4–8.
- [3] M.P. Searle, Cooling history, erosion, exhumation, and kinematics of the Himalaya-Karakoram-Tibet orogenic belt, in: A. Yin, T.M. Harrison (Eds.), *The Tectonic Evolution of Asia*, Cambridge University Press, New York, 1996, pp. 110–137.
- [4] P. Le Fort, Evolution of the Himalaya, in: A. Yin, T.M. Harrison (Eds.), *The Tectonic Evolution of Asia*, Cambridge University Press, New York, 1996, pp. 95–109.
- [5] A. Yin, T.M. Harrison, Geologic evolution of the Himalayan-Tibetan orogen, *Annu. Rev. Earth Planet. Sci.* 28 (2000) 211–280.
- [6] B.C. Burchfiel, Z. Chen, K.V. Hodges, Y. Liu, L.H. Royden, C. Deng, J. Xu, The South Tibetan Detachment System, Himalayan Orogen: Extension contemporaneous with and parallel to shortening in a collisional mountain belt, *Geol. Soc. Am. Spec. Pap.* 269 (1992) 1–41.
- [7] T.M. Harrison, P. Copeland, W.S.F. Kidd, O.M. Lovera, Activation of the Nyainqentanghla shear zone: Implications for uplift of the southern Tibetan Plateau, *Tectonics* 14 (1995) 658–676.
- [8] K.V. Hodges, Tectonics of the Himalaya and southern Tibet from two perspectives, *Geol. Soc. Am. Bull.* 112 (2000) 324–350.
- [9] R.D. Lawrence, S.H. Khan, K.A. Dejong, A. Farah, R.S. Yeats, Thrust and strike slip fault interaction along the Chaman transform zone, Pakistan, in: K.R. McClay, N.J. Price (Eds.), *Thrust and nappe tectonics*, *Geol. Soc. Spec. Pub.* 9, London, 1981, pp. 363–370.
- [10] D.D. Schelling, Frontal structural geometries and detachment tectonics of the northeastern Karachi arc, southern Kirthar Range, Pakistan, *Geol. Soc. Am. Spec. Pap.* 328 (1999) 287–302.
- [11] J.F. Ni, M. Guzman-Speziale, M. Bevis, W.E. Holt, T.C. Wallace, W.R. Seager, Accretionary tectonics of Burma and the three-dimensional geometry of the Burma subduction zone, *Geology* 17 (1989) 68–71.
- [12] P.H. Leloup, R. Lacassin, P. Tapponnier, U. Schärer, D. Zhong, X. Liu, L. Zhang, S. Ji, P.T. Trinh, The Ailao Shan-Red River shear zone (Yunnan, China), Tertiary transform boundary of Indochina, *Tectonophysics* 251 (1995) 3–84.
- [13] E. Wang, B.C. Burchfiel, Interpretation of Cenozoic tectonics in the right-lateral accommodation zone between the Ailao Shan shear zone and the eastern Himalayan syntaxis, *Int. Geol. Rev.* 39 (1997) 191–219.
- [14] S. Tonarini, I. Villa, F. Oberli, M. Meier, D.A. Spencer, U. Pognante, J.G. Ramsay, Eocene age of eclogite metamorphism in the Pakistan Himalaya Implications for India-Eurasian collision, *Terra Nova* 5 (1993) 13–20.
- [15] L. Ding, D. Zhong, Metamorphic characteristics and geotectonic implications of the high-pressure granulites from Namche Barwa, eastern Tibet, *Sci. China* 42 (1999) 491–505.
- [16] M.A. Poage, C.P. Chamberlain, D. Craw, Massif-wide metamorphism and fluid evolution at Nanga Parbat, northern Pakistan, *Am. J. Sci.* 300 (2000) 463–482.
- [17] P.K. Zeitler, Cooling history of the NW Himalaya, Pakistan, *Tectonics* 4 (1985) 127–151.
- [18] D.A. Schneider, M.A. Edwards, W.S.F. Kidd, M.A. Khan, L. Seeber, P.K. Zeitler, Tectonics of Nanga Parbat, western Himalaya Synkinematic plutonism within the doubly vergent shear zones of a crustal-scale pop-up structure, *Geology* 27 (1999) 999–1002.
- [19] M.A. Edwards, W.S.F. Kidd, M.A. Khan, D.A. Schneider, Tectonics of the SW margin of the Nanga Parbat-Haramosh massif, in: M.A. Khan, P.J. Treloar, M.P. Searle, M.Q. Jan, (Eds.), *Tectonics of the Nanga Parbat syntaxis and the Western Himalaya*, *Geol. Soc. Spec. Pub.* 170, London, 2001, pp. 77–100.
- [20] D. Zhong, L. Ding, Discovery of high-pressure basic granulites in Namjagbarwa area, Tibet, China, *Chin. Sci. Bull.* 41 (1996) 87–88.
- [21] D. Zhong, L. Ding, Raising process of the Qinghai-Xizang (Tibet) plateau and its mechanism, *Sci. China* 39 (1996) 369–379.
- [22] Z.G. Zhang, Y.H. Liu, T.W. Qnag, H.X. Yang, B.C. Xu, Geology of the Namche Barwa Region, Chinese Science Press, Beijing, 1992, 185 pp.
- [23] A. Yin, T.M. Harrison, F.J. Ryerson, W.J. Chen, W.S.F. Kidd, P. Copeland, Tertiary structural evolution of the Gangdese thrust system in southeastern Tibet, *J. Geophys. Res.* 99 (1994) 18175–18201.
- [24] A. Yin, T.M. Harrison, M.A. Murphy, M. Grove, S. Nie, F.J. Ryerson, X.F. Wang, Z.L. Chen, Tertiary deformation history of southeastern and southwestern Tibet during the Indo-Asian collision, *Geol. Soc. Am. Bull.* 111 (1999) 1644–1664.
- [25] T.M. Harrison, A. Yin, M. Grove, O.M. Lovera, F.J. Ryerson, X. Zhou, The Zedong Window: A record of

- superposed Tertiary convergence in southeastern Tibet, *J. Geophys. Res.* 105 (2000) 19211–19230.
- [26] V.C. Thakur, A.K. Jain, Some observations on deformation, metamorphism and tectonic significance of the rocks of some parts of the Mishimi hills, Lohit District (Nefa), *Himal. Geol.* 5 (1975) 339–364.
- [27] S. Singh, Geology and tectonics of the Eastern Syntaxial Bend, Arunachal Himalaya, *J. Himal. Geol.* 4 (1993) 149–163.
- [28] X. Zheng, C. Chang, A preliminary note on the tectonic features of the lower Yalu-Tsangpo river region, *Sci. Geol. Sin.* 2 (1979) 116–126.
- [29] R. Armijo, P. Tapponnier, J.L. Mercier, T.-L. Han, Quaternary extension in southern Tibet: Field observations and tectonic implications, *J. Geophys. Res.* 91 (1986) 13803–13872.
- [30] J.P. Burg, G.M. Chen, Tectonics and structural zonation of southern Tibet, China, *Nature* 311 (1984) 219–223.
- [31] J.B. Paces, J.D. Miller, Precise U-Pb age of Duluth Complex and related mafic intrusions, northeastern Minnesota: Geochronological insights into physical, petrogenetic, paleomagnetic, and tectonomagmatic processes associated with the 1.1 Ga midcontinent rift system, *J. Geophys. Res.* 98 (1993) 13997–14013.
- [32] J.S. Stacey, J.D. Kramers, Approximation of terrestrial lead isotope evolution by a two-stage model, *Earth Planet. Sci. Lett.* 26 (1975) 207–221.
- [33] X. Quidelleur, M. Grove, O.M. Lovera, T.M. Harrison, A. Yin, Thermal evolution and slip history of the Renbuzedong Thrust, southeastern Tibet, *J. Geophys. Res.* 102 (1997) 2659–2679.
- [34] S. Wang, H. Sang, S. Hu, $^{40}\text{Ar}/^{39}\text{Ar}$ age determination using 49-2 reactor and $^{40}\text{Ar}/^{39}\text{Ar}$ age spectrum for amphibolite from Qianan, China, *Acta Petrol. Sin.* 2 (1985) 35–44.
- [35] S. Wang, Constraints of chlorine on $^{40}\text{Ar}/^{39}\text{Ar}$ dating and calculation of precise $^{40}\text{Ar}/^{39}\text{Ar}$ ages, *Sci. Geol. Sin.* 27 (1992) 369–378.
- [36] R. Armijo, P. Tapponnier, H. Tonglin, Late Cenozoic right-lateral strike-slip faulting in southern Tibet, *J. Geophys. Res.* 94 (1989) 2787–2838.
- [37] M.A. Edwards, T.M. Harrison, When did the roof collapse? Late Miocene north–south extension in the high Himalaya revealed by Th-Pb monazite dating of the Khula Kangri granite, *Geology* 25 (1997) 543–546.
- [38] C. Wu, K.D. Nelson, G. Wortman, S.D. Samson, Y. Yue, J. Li, W.S.F. Kidd, M.A. Edwards, Yadong cross structure and South Tibetan detachment in the east central Himalaya (89 degrees–90 degrees E), *Tectonics* 17 (1998) 28–45.
- [39] M.A. Murphy, T.M. Harrison, Relationship between leucogranites and the Qomolangma detachment in the Rongbuk Valley, south Tibet, *Geology* 27 (1999) 831–834.
- [40] G. Mahood, W. Hildreth, Large partition coefficients for trace elements in high-silica rhyolites, *Geochim. Cosmochim. Acta* 47 (1983) 11–30.
- [41] H.R. Rollinson, B.F. Windley, Selective elemental depletion during metamorphism of Archaean granulites, Scourie, NW Scotland, *Contrib. Mineral. Petrol.* 72 (1980) 257–263.
- [42] U. Schärer, C.J. Allègre, The Palung granite (Himalaya); high-resolution U-Pb systematics in zircon and monazite, *Earth Planet. Sci. Lett.* 63 (1983) 432–432.
- [43] R.-H. Xu, U. Schärer, C.J. Allègre, Magmatism and metamorphism in the Lhasa block (Tibet): a geochronological study, *J. Geol.* 93 (1985) 41–57.
- [44] P.K. Zeitler, J.F. Sutter, I.S. Williams, R. Zartman, R.A.K. Tahirkheli, Geochronology and temperature history of the Nanga Parbat-Harmosh Massif, Pakistan, *Geol. Soc. Am. Spec. Pap.* 232 (1989) 1–22.
- [45] P.G. DeCelles, G.E. Gehrels, J. Quade, B. LaReau, M. Spurlin, Tectonic implications of U-Pb zircon ages of the Himalayan orogenic belt in Nepal, *Science* 288 (2000) 497–499.
- [46] P. Kapp, A. Yin, C.E. Manning, M.A. Murphy, T.M. Harrison, M. Spurlin, L. Ding, X. Deng, C. Wu, Blueschist-bearing metamorphic core complexes in the Qiangtang block reveal deep crustal structure of northern Tibet, *Geology* 28 (2000) 19–22.
- [47] I. McDougall, T.M. Harrison, *Geochronology and Thermochronology by the $^{40}\text{Ar}/^{39}\text{Ar}$ Method*, Oxford University Press, New York, 1999, 261 pp.
- [48] W. Zhao, K.D. Nelson, Project INDEPTH Team, Deep seismic reflection evidence for continental underthrusting beneath southern Tibet, *Nature* 366 (1993) 557–579.
- [49] K.D. Nelson, W. Zhao, L.D. Brown, J. Kuo, J. Che, X. Liu, S.L. Klemperer, Y. Makovsky, R. Meissner, J. Mechie, R. Kind, F. Wenzel, J. Ni, J. Nabelek, L. Chen, H. Tan, W. Wei, A.G. Jones, J. Booker, M. Unsworth, W.S.F. Kidd, M. Hauck, D. Alsdorf, A. Ross, M. Cogan, C. Wu, E. Sandvol, M. Edwards, Partially molten middle crust beneath southern Tibet: Synthesis of Project INDEPTH results, *Nature* 274 (1996) 1684–1688.
- [50] P.J. O'Brien, N. Zotov, R. Law, M.A. Khan, M.Q. Jan, Coesite in Himalayan eclogite and implications for models of India-Asia collision, *Geology* 29 (2001) 435–438.
- [51] D.B. Rowley, Age of initiation of collision between India and Asia: A review of stratigraphic data, *Earth Planet. Sci. Lett.* 145 (1996) 1–13.
- [52] S. Guillot, M. Cosca, P. Allemand, P. Le Fort, Contrasting metamorphic and geochronologic evolution along the Himalayan Belt, in: A. MacFarlane, R.B. Sorkhabi, J. Quade (Eds.), *Himalaya and Tibet, Mountain Roots to Mountain Tops*, *Geol. Soc. Am. Spec. Pap.* 328, Boulder, CO, 1999, pp. 117–128.
- [53] P.K. Zeitler, C.P. Chamberlain, H.A. Smith, Synchronous anatexis, metamorphism, and rapid denudation at Nanga Parbat (Pakistan Himalaya), *Geology* 21 (1993) 347–350.
- [54] C.P. Chamberlain, P.K. Zeitler, D.E. Barnett, D. Winslow, S.R. Poulson, T. Leahy, J.E. Hammer, Active hydrothermal systems during the recent uplift of Nanga Parbat, Pakistan Himalaya, *J. Geophys. Res.* 100 (1995) 439–453.